

BCSJ Award Article

BDT-TTP-Based π Conductors Containing Divalent Magnetic and Non-Magnetic Inorganic Anions, $[M^{II}Cl_4]^{2-}$ (M = Co, Mn, Zn)

Tetsuro Kusamoto,[1] Emiko Fujiwara,[1] Akiko Kobayashi,*[1] Hengbo Cui,[2] Takeo Otsuka,[2] Yoshinori Okano,[2] Hideki Fujiwara,[2] and Hayao Kobayashi[2]

[1]Research Centre for Spectrochemistry, Graduate School of Science, The University of Tokyo, 7-3-1 Hongo, Bunkyo-ku, Tokyo 113-0033

[2]Institute for Molecular Science and CREST, JST, 38 Nishigounaka, Myodaiji, Okazaki 444-8585

Received November 29, 2005; E-mail: akiko@chem.s.u-tokyo.ac.jp

Three BDT-TTP [2,5-bis(1,3-dithiol-2-ylidene)-1,3,4,6-tetrathiapentalene] salts, $(BDT\text{-}TTP)_3[M^{II}Cl_4](EtOH)_x$ (M = Co, Mn, and Zn; $x \approx 1.0$) were prepared. These salts are almost isostructural to one another. The crystals are composed of BDT-TTP columns, "BDT-TTP tapes" that occupy the interstitial positions between BDT-TTP columns, $[M^{II}Cl_4]^{2-}$ anions and the crystal solvents, respectively. These salts showed weakly metallic conducting behavior down to about 150 K. At low temperature, the resistivities increased gradually with decreasing temperature, but the systems retained fairly high conductivities even at around 30 K. The $[Zn^{II}Cl_4]^{2-}$ salt indicated temperature independent paramagnetism down to low temperature. While the susceptibilities of the $[Co^{II}Cl_4]^{2-}$ and $[Mn^{II}Cl_4]^{2-}$ salts showed the coexistence of π conduction electrons and localized high-spins of the magnetic Co^{II} and Mn^{II} atoms, no significant π–d interaction was observed. Band structure calculations were performed with taking account of the possibility of inhomogeneous distribution of π electrons over the crystallographically independent three BDT-TTP molecules. The system has wide and narrow one-dimensional bands that originate from BDT-TTP columns and tapes, respectively. However, due to the interaction between BDT-TTP columns and tapes, the system gave a unique two-dimensional electronic band. The calculated energy dispersion curves were consistent with the weakly metallic behavior of the systems.

Recently, organic–inorganic hybrid molecular materials that consist of organic conduction layers and inorganic magnetic layers have attracted considerable interest because they are regarded as suitable systems to develop multi-functional molecular systems such as magnetic conductors.[1] Typically, these magnetic organic conductors are divided into two groups according to the magnitude of the coupling between inorganic and organic parts. One group contains both the first paramagnetic superconductor, β''-$(BEDT\text{-}TTF)_4(H_3O)Fe^{III}(C_2O_4)_3(C_6H_5CN)$ [BEDT-TTF = bis(ethylenedithio)tetrathiafulvalene],[2] and the first ferromagnetic organic conductor, $(BEDT\text{-}TTF)_3[Mn^{II}Cr^{III}(C_2O_4)_3]$.[3] Needless to say, in these salts, π electrons in the donor layer are responsible for the conducting properties and d electrons of the anions are responsible for magnetic properties. However, the conducting part and magnetic part are almost independent of each other. The other group contains a series of the BETS conductors with metal halide anions $(BETS)_2M^{III}X_4$ salts [BETS = bis(ethylenedithio)tetraselenafulvalene; M = Fe and Ga; X = Cl and Br], including the systems[4] in which the coupling of conducting π electrons and magnetic d spins (π–d interaction) produces intriguing "dual-active phenomena" such as field-induced superconductivity,[5] superconductor-to-insulator transitions,[6] metamagnetic switching of the antiferromagnetic superconducting state,[7] and so on.

Though several important magnetic conductors have been discovered so far, the research on the development of magnetic organic metals, especially such as dual-active magnetic conductors, is of course still insufficient. We have tried to prepare the organic conductors based on π-donor BDT-TTP molecules[8] (Chart 1) and magnetic anions because similar to BETS, BDT-TTP has produced many organic conductors with metallic behavior down to liquid helium temperature and therefore will provide a chance of the coexistence of mutually interacting π metal electrons and localized magnetic moments of transition-metal atoms.[9] However, unlike BETS systems, single crystals of BDT-TTP salts with typical magnetic monoanions such as $[Fe^{III}Cl_4]^-$ and $[Fe^{III}Br_4]^-$ could not be prepared. On the other hand, crystals with divalent magnetic anions $[M^{II}Cl_4]^{2-}$

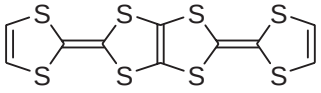

BDT-TTP

Chart 1.

Published on the web April 7, 2006; DOI: 10.1246/bcsj.79.527

Table 1. Crystallographic Data of (BDT-TTP)$_3$[M^{II}Cl$_4$](EtOH)$_x$ (M = Co, Mn, and Zn; $x \approx 1.0$)

	(BDT-TTP)$_3$[Co^{II}Cl$_4$](EtOH)$_x$	(BDT-TTP)$_3$[Mn^{II}Cl$_4$](EtOH)$_x$	(BDT-TTP)$_3$[Zn^{II}Cl$_4$](EtOH)$_x$
Formula	$C_{32}H_{18}S_{24}CoCl_4O$	$C_{32}H_{18}S_{24}MnCl_4O$	$C_{32}H_{18}S_{24}ZnCl_4O$
Habit	black, needle	black, needle	black, needle
Formula weight	1388.81	1384.82	1395.27
Crystal system	monoclinic	monoclinic	monoclinic
Space group	$C2/m$	$C2/m$	$C2$
a/Å	39.38(4)	39.84(3)	39.62(2)
b/Å	19.06(2)	19.04(2)	19.027(9)
c/Å	6.857(7)	6.851(6)	6.832(4)
β/deg	97.58(2)	97.22(1)	97.30(2)
V/Å^3	5100.9(87)	5155.4(74)	5109.3(42)
Z	4	4	4
μ/cm^{-1}	1.558	1.464	1.700
$F(000)$	2736.00	2728.00	2748.00
max 2θ	63.0	62.0	62.0
trans factors min	0.773	0.620	0.728
trans factors max	0.969	0.971	0.967
No. of reflections			
Measured	7608	7643	29544
Observed (used)	1439	1992	2744
D_{calcd}/g cm^{-3}	1.778	1.754	1.784
R[a)]	0.0960	0.0840	0.1010
R_w[a)]	0.1010	0.0890	0.1240
GOF	1.178	1.144	1.033

a) $R = \Sigma||F_0| - |F_c||/\Sigma|F_0|$; $R_w = [\Sigma w(|F_0| - |F_c|)^2/\Sigma wF_0{}^2]^{1/2}$.

(M = Co and Mn) and non-magnetic anion [Zn^{II}Cl$_4$]$^{2-}$ were obtained. Though several examples of organic conductors involving magnetic metal halide dianions have been reported,[10,11] it will be important to explore further new magnetic organic conductors containing magnetic dianions. In this paper, we report the crystal and band structures and electric and magnetic properties of BDT-TTP conductors with [M^{II}Cl$_4$]$^{2-}$ (M = Co, Mn, and Zn).

Experimental

Reagents. BDT-TTP was synthesized according to the method reported by Misaki et al.[8] [(C$_2$H$_5$)$_4$N]$_2$[M^{II}Cl$_4$] (M = Co, Mn, and Zn) was prepared by mixing [(C$_2$H$_5$)$_4$N]Cl and M^{II}Cl$_2$ in hot ethanol (EtOH), recrystallized three times from EtOH solution, dried in vacuo, and used for the electrocrystallization. Chlorobenzene (PhCl) used for electrocrystallizations was washed with concentrated sulfuric acid and then with aqueous sodium hydrogencarbonate solution and water, followed by drying with calcium chloride, and was distilled with diphosphorus pentaoxide under an argon atmosphere. EtOH for electrocrystallizations was distilled over magnesium ethoxide under an argon atmosphere. Both solvents were stored at room temperature.

Electrocrystallization. Single crystals were grown by an ordinary electrochemical oxidation method. An H-shaped glass cell with two platinum wires, which were used as electrodes, was filled with 11 mL of an EtOH–PhCl (v:v = 1:10) solution containing 2.5 mg (6.6 mmol) of BDT-TTP and 25–30 mg (54–65 mmol) of the tetraethylammonium salt [(C$_2$H$_5$)$_4$N]$_2$[M^{II}Cl$_4$] (M = Co, Mn, and Zn). A constant voltage of 2.0 V was applied at room temperature. Needle-shaped black crystals were obtained after 2 weeks. X-ray crystal structure determinations have revealed the existence of heavily disordered EtOH, which was confirmed by the IR spectra of the crystalline powder samples that show a broad OH stretching vibration around 3200–3400 cm^{-1}. The elementary analysis could not be performed since crystals with another shape were at the same time grown on the platinum electrode.

Crystallographic Data Collection and Structure Determination. The crystal structures of (BDT-TTP)$_3$[Co^{II}Cl$_4$](EtOH)$_x$ ($x \approx 1.0$) and (BDT-TTP)$_3$[Mn^{II}Cl$_4$](EtOH)$_x$ ($x \approx 1.0$) were analyzed at room temperature on a Rigaku/MSC MERCURY CCD X-ray system. Graphite-monochromated Mo Kα radiation (λ = 0.71070 Å) was used. The crystal structure analysis of (BDT-TTP)$_3$[Zn^{II}Cl$_4$](EtOH)$_x$ ($x \approx 1.0$) was performed by using a Rigaku AFC-8 MERCURY CCD X-ray system. A confocal X-ray mirror system (λ = 0.71070 Å) was used. The sizes of the crystals were 0.30 × 0.10 × 0.05 mm^3 [Co^{II}Cl$_4$]$^{2-}$ salt, 0.25 × 0.10 × 0.05 mm^3 [Mn^{II}Cl$_4$]$^{2-}$ salt, and 0.25 × 0.10 × 0.05 mm^3 [Zn^{II}Cl$_4$]$^{2-}$ salt. Though the quality of the crystals was not sufficient, especially in [Zn^{II}Cl$_4$]$^{2-}$ salt, the structure analyses were successfully completed. All the calculations were performed using the crystallographic software package, CrystalStructure.[12] Non-hydrogen atoms were refined anisotropically for the [Mn^{II}Cl$_4$]$^{2-}$ salts, while the atoms except for hydrogen and carbon atoms were refined anisotropically and carbon atoms were refined isotropically for the [Co^{II}Cl$_4$]$^{2-}$ and [Zn^{II}Cl$_4$]$^{2-}$ salts. The positions of the hydrogen atoms were determined from the geometric conditions and were fixed in the refinement. Table 1 summarizes the experimental details and the results of the crystal structure analyses of (BDT-TTP)$_3$[M^{II}Cl$_4$](EtOH)$_x$ (M = Co, Mn, and Zn; $x \approx 1.0$). Crystallographic data have been deposited with Cambridge Crystallographic Data Centre: Deposition numbers CCDC-253498 (M = Co), CCDC-253499 (M = Zn), and CCDC-253500 (M = Mn) for (BDT-TTP)$_3$[M^{II}Cl$_4$](EtOH)$_x$ ($x \approx 1.0$). Copies of the data can be obtained free of charge via http://www.ccdc.cam.ac.uk/conts/retrieving.html (or from the Cambridge Crystallographic Data Centre, 12, Union Road, Cambridge, CB2 1EZ, UK; Fax: +44 1223 336033; e-mail: deposit@ccdc.cam.ac.uk).

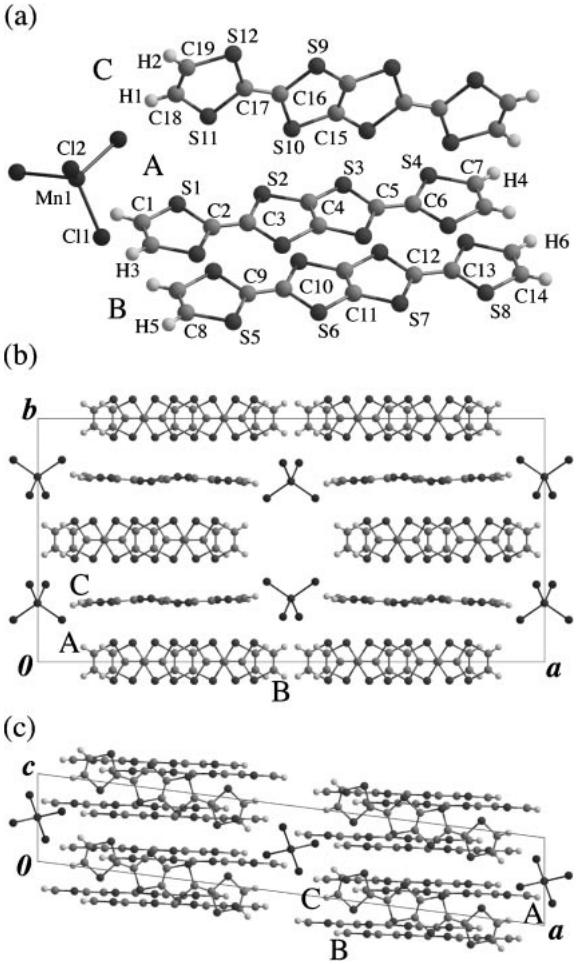

Fig. 1. (a) Crystallographically independent molecules of (BDT-TTP)[$Mn^{II}Cl_4$](EtOH)$_x$ ($x \approx 1.0$). (b) Crystal structure of (BDT-TTP)$_3$[$Mn^{II}Cl_4$](EtOH)$_x$ ($x \approx 1.0$) projected onto the *ab*-plane. (c) Crystal structure of (BDT-TTP)$_3$-[$Mn^{II}Cl_4$](EtOH)$_x$ ($x \approx 1.0$) projected onto the *ac*-plane. The crystal structure of (BDT-TTP)$_3$[$Co^{II}Cl_4$](EtOH)$_x$ ($x \approx 1.0$) is isostructural to that of (BDT-TTP)$_3$[$Mn^{II}Cl_4$]-(EtOH)$_x$ ($x \approx 1.0$). The atomic positions of EtOH are heavily disordered and are omitted for clarify. The donors A, B, and C are crystallographically independent BDT-TTP molecules, respectively.

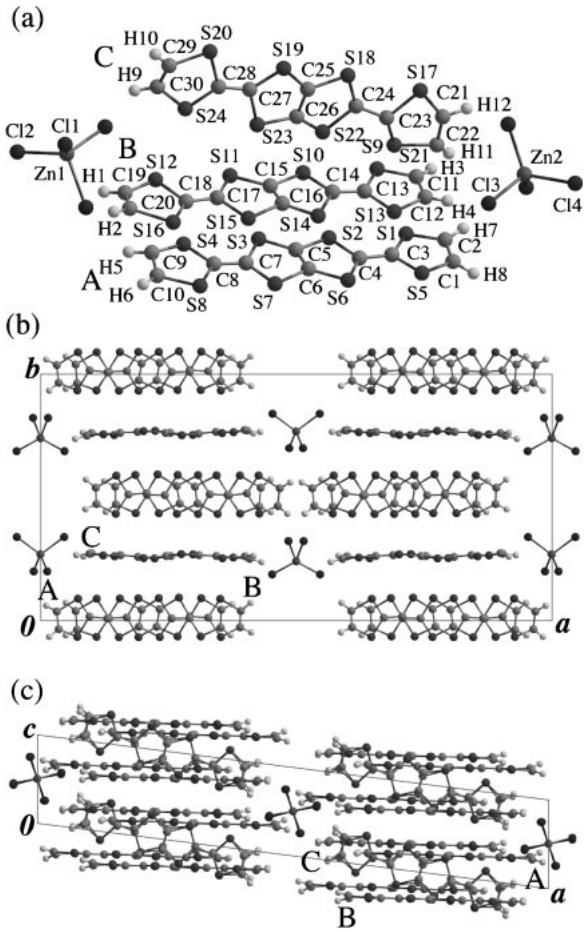

Fig. 2. (a) Crystallographically independent molecules of (BDT-TTP)$_3$[$Zn^{II}Cl_4$](EtOH)$_x$ ($x \approx 1.0$). (b) Crystal structure of (BDT-TTP)$_3$[$Zn^{II}Cl_4$](EtOH)$_x$ ($x \approx 1.0$) projected onto the *ab*-plane. (c) Crystal structure of (BDT-TTP)$_3$-[$Zn^{II}Cl_4$](EtOH)$_x$ ($x \approx 1.0$) projected onto the *ac*-plane. The heavy disordered EtOH molecules are omitted for clarify. The donors A, B, and C are crystallographically independent BDT-TTP molecules, respectively.

Electrical Resistivity Measurement. The four-probe electrical resistivity measurements were performed on the $[M^{II}Cl_4]^{2-}$ salts (M = Co, Mn, and Zn) down to liquid helium temperature by using a Huso Electro Chemical System HECS 944C multi-channel 4-terminal conductometer. Electrical contacts were achieved with gold wire (15 $\mu m\phi$) and gold paste.

Static Magnetic Susceptibility Measurement. The magnetic susceptibilities were measured using a Quantum Design MPMS-7XL SQUID magnetometer in the temperature range from 2.0 to 300 K at 1 Tesla for the $[Co^{II}Cl_4]^{2-}$ and the $[Mn^{II}Cl_4]^{2-}$ salts, and at 2 Tesla for the $[Zn^{II}Cl_4]^{2-}$ salt. The samples were wrapped with clean aluminum foil, whose magnetic susceptibility was separately measured and subtracted. The data was corrected for the diamagnetic contribution estimated from Pascal's constants [$\chi^{dia} = -6.44 \times 10^{-4}$ emu mol^{-1} for (BDT-TTP)$_3$[$Co^{II}Cl_4$](EtOH)$_x$ ($x \approx 1.0$), $\chi^{dia} = -6.46 \times 10^{-4}$ emu mol^{-1} for (BDT-TTP)$_3$[$Mn^{II}Cl_4$]-(EtOH)$_x$ ($x \approx 1.0$), and $\chi^{dia} = -6.46 \times 10^{-4}$ emu mol^{-1} for (BDT-TTP)$_3$[$Zn^{II}Cl_4$](EtOH)$_x$ ($x \approx 1.0$)].

Band Structure Calculations. The overlap integrals and band structures were calculated by a tight-binding method based on the extended Hückel approximation. Slater-type atomic orbitals were used. The parameters of the atomic orbitals are the same as those used previously in (BDT-TTP)$_2$I.[13] The exponent ξ and the ionization potential (eV) are: S 3s, 2.122, −20.0; S 3p, 1.827, −11.0; S 3d, 1.500, −5.4; C 2s, 1.625, −21.4; C 2p, 1.625, −11.4; H 1s, 1.0, −13.6.

Results and Discussion

Crystal Structures of the $[M^{II}Cl_4]^{2-}$ (M = Co, Mn, and Zn) Salts. Single-crystal X-ray structure analyses revealed that the crystal structures of the $[M^{II}Cl_4]^{2-}$ (M = Co and Mn) salts are almost isostructural to one another (Fig. 1). The $[Co^{II}-Cl_4]^{2-}$ and $[Mn^{II}Cl_4]^{2-}$ salts have three independent halves of BDT-TTP molecules [donors A, B, and C, shown in Fig. 1a], and half of a crystallographically independent $[M^{II}Cl_4]^{2-}$ anion. The electron density map suggests the existence of a

Table 2. Averaged Bond Lengths (Å) of BDT-TTF Molecules[a)]

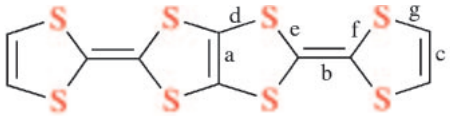

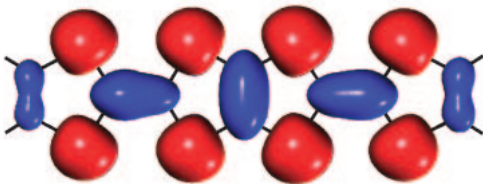

Compound	Donor	a	b	c	d	e	f	g
$(BDT\text{-}TTP)_3[Mn^{II}Cl_4](EtOH)_x$	A	1.321	1.394	1.289	1.742	1.760	1.731	1.755
	B	1.398	1.363	1.324	1.727	1.744	1.743	1.739
	C	1.417	1.390	1.337	1.725	1.769	1.740	1.738
$(BDT\text{-}TTP)_3[Co^{II}Cl_4](EtOH)_x$	A	1.323	1.400	1.327	1.748	1.762	1.747	1.738
	B	1.395	1.352	1.247	1.727	1.754	1.738	1.777
	C	1.379	1.411	1.322	1.733	1.765	1.739	1.736
$(BDT\text{-}TTP)_3[Zn^{II}Cl_4](EtOH)_x$	A	1.323	1.375	1.383	1.751	1.765	1.730	1.732
	B	1.367	1.392	1.370	1.740	1.741	1.754	1.741
	C	1.414	1.418	1.345	1.726	1.764	1.743	1.757
BDT-TTP[8d]		1.327	1.336	1.332	1.750	1.769	1.760	1.733
Optimized structure (PM3)		1.366	1.351	1.342	1.736	1.767	1.765	1.741
$(BDT\text{-}TTP)_2I$ (Ref. 13)	A	1.346	1.356	1.320	1.736	1.767	1.744	1.745
$(BDT\text{-}TTP)_3I$ (Ref. 13)	A	1.353	1.351	1.324	1.735	1.754	1.754	1.739
	B	1.348	1.359	1.332	1.738	1.755	1.754	1.747
	C	1.320	1.335	1.323	1.745	1.755	1.763	1.735
	D	1.340	1.346	1.324	1.749	1.768	1.763	1.745
	E	1.317	1.335	1.304	1.751	1.775	1.757	1.738
	F	1.330	1.352	1.331	1.756	1.771	1.760	1.742

a) The molecules are assumed to have D_{2h} symmetry. HOMO is also presented.

heavily disordered crystal solvent around the inversion center, but their atomic positions could be hardly identified. Since the IR spectra of $(BDT\text{-}TTP)_3[M^{II}Cl_4](solvent)_x$ showed OH stretching vibration but no Ph–Cl vibration, the possibility of the inclusion of PhCl was excluded. Based on the comparisons of the unit cell volumes of the crystals of neutral BETS and BDT-TTP molecules,[6c,11] κ-$(BETS)_4[Co^{II}Cl_4](EtOH)$, $(BETS)_2[Co^{II}Cl_4]$, and $(BDT\text{-}TTP)[Co^{II}Cl_4](EtOH)_x$, and the X-ray structure refinements, the x-value was roughly estimated to be about 1.0.[14]

For the $[Zn^{II}Cl_4]^{2-}$ salt, the crystal structure was almost the same as those of $[M^{II}Cl_4]^{2-}$ (M = Co and Mn) salts, but there were three crystallographically independent BDT-TTP molecules [donors A, B, and C, shown in Fig. 2a], two independent halves of $[Zn^{II}Cl_4]^{2-}$ anions, and disordered EtOH (Fig. 2). We tried to refine the structure of the $[Zn^{II}Cl_4]^{2-}$ salt using the space group of $C2/m$; however, we could not obtain good results. Thus, we selected the space group of $C2$ for the $[Zn^{II}Cl_4]^{2-}$ salt.

The average distances of the C=C and C–S bonds of the donor molecules in these salts are listed in Table 2, where the optimized bond lengths of the neutral BDT-TTP molecule and previously reported bond lengths of $(BDT\text{-}TTP)_nI$ ($n = 2$ and 3) are also listed.[13,15] Unlike the BEDT-TTF molecule with a slightly bent structure in its neutral state,[16] the optimized structure of the neutral BDT-TTP is almost planar. Interestingly, in the optimized structure of the neutral BDT-TTP, the C=C bonds (*a*) of the central TTP part are longer than the *outer* C=C bonds (*c*), which suggests a large π population on the central part of the molecule. However, such a tendency of the bond lengths is not clear in the real crystals. On the other hand, the *inner* C–S bond lengths in the TTF skeleton [bonds *e* and *f* (see Table 2)] are a little longer than those of the *outer* C–S bonds (*d* and *g*), and this tendency is also observed in most of the BDT-TTP salts despite the insufficient accuracy of structure analyses. It is well known that in the TTF-like π-donor molecules, the C=C bonds tend to be shortened while the C–S bonds tend to be lengthened by the oxidation of the molecule. This is of course due to the symmetry of the highest occupied molecular orbital (HOMO) of the TTF-like π-donor molecule, which has bonding and antibonding characters on the C=C and C–S bonds, respectively (see HOMO shown in Table 2). Although the accuracy of the bond lengths was not sufficient to observe such a tendency, there is a possibility that the formal charge of molecule C will be nearly 0 and those of molecules A and B will be +1.

Donors A and B stack along the *c* axis to form an almost uniform column with a ring-over-bond type stacking mode (Fig. 3). The intermolecular interplanar distances are 3.44 Å (A···B′) and 3.41 Å (A···B) for the $[Co^{II}Cl_4]^{2-}$ salt, 3.44 Å

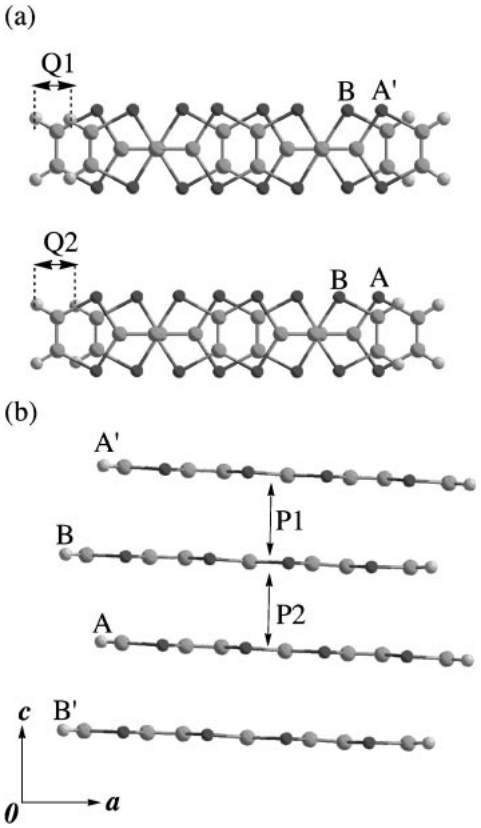

Fig. 3. (a) Overlap mode of the donor molecules of (BDT-TTP)$_3$[$M^{II}Cl_4$](EtOH)$_x$ (M = Co, Mn, and Zn; $x \approx 1.0$) projected along the *c* axis. Slip distances (Å): 1.33 (Q1) and 1.55 (Q2) for the [$Co^{II}Cl_4$]$^{2-}$ salt, 1.35 (Q1) and 1.58 (Q2) for the [$Mn^{II}Cl_4$]$^{2-}$ salt, and 1.34 (Q1) and 1.60 (Q2) for the [$Zn^{II}Cl_4$]$^{2-}$ salt. (b) Donor stacking of (BDT-TTP)$_3$[$M^{II}Cl_4$](EtOH)$_x$ (M = Co, Mn, and Zn; $x \approx 1.0$) viewed along the *b* axis. Intermolecular interplanar distances (Å): 3.44 (P1) and 3.41 (P2) for the [$Co^{II}Cl_4$]$^{2-}$ salt, 3.44 (P1) and 3.40 (P2) for the [$Mn^{II}Cl_4$]$^{2-}$ salt, and 3.42 (P1) and 3.40 (P2) for the [$Zn^{II}Cl_4$]$^{2-}$ salt.

(A···B′) and 3.40 Å (A···B) for the [$Mn^{II}Cl_4$]$^{2-}$ salt, and 3.42 Å (A···B′) and 3.40 Å (A···B) for the [$Zn^{II}Cl_4$]$^{2-}$ salt. The slip distances along the long axis of the donors that form the columns are 1.33 Å (A···B) and 1.55 Å (A···B′) for the [$Co^{II}Cl_4$]$^{2-}$ salt, 1.35 Å (A···B) and 1.58 Å (A···B′) for the [$Mn^{II}Cl_4$]$^{2-}$ salt, and 1.34 Å (A···B) and 1.60 Å (A···B′) for the [$Zn^{II}Cl_4$]$^{2-}$ salt. As mentioned above, donors C are located between the columns and arranged in a side-by-side manner to form a unique one-dimensional "BDT-TTP tape" along the *c* axis and the molecular plane of donor C is approximately perpendicular to those of donors A and B (Fig. 4). There are S···S contacts shorter than the sum of the van der Waals radii (3.7 Å) between the donors (Table 3 and Figs. 4 and 5). The [$M^{II}Cl_4$]$^{2-}$ (M = Co, Mn, and Zn) anion takes a tetrahedral structure and is located on the 2-fold axis and surrounded by four BDT-TTP columns, two BDT-TTP tapes, and crystal solvents. The shortest M···M distances along the *c* axis are 6.85(7) Å for the [$Co^{II}Cl_4$]$^{2-}$ salt, 6.85(1) Å for the [$Mn^{II}Cl_4$]$^{2-}$ salt, and 6.83(2) Å [Zn(1)···Zn(1)] and 6.83(2) Å [Zn(2)···Zn(2)] for the [$Zn^{II}Cl_4$]$^{2-}$ salt. The shortest Cl···Cl distances are 3.481(2) Å [Cl(2)···Cl(2)]

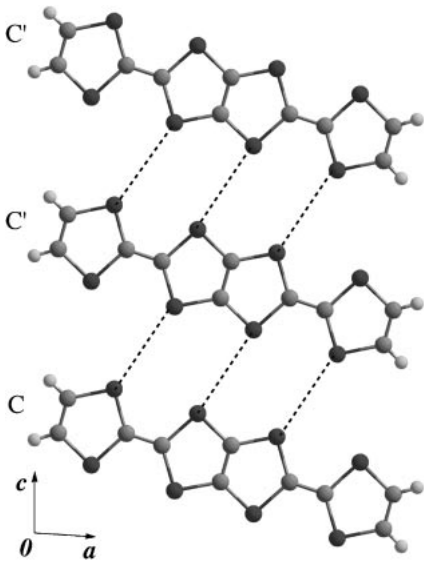

Fig. 4. Side-by-side arrangement (tape structure) of molecule C (see Figs. 1 and 2). The close S···S distances are presented as dotted lines. The shortest S···S distance is 3.756 Å for the [$Co^{II}Cl_4$]$^{2-}$ salt, 3.732 Å for the [$Mn^{II}Cl_4$]$^{2-}$ salt, and 3.724 Å for the [$Zn^{II}Cl_4$]$^{2-}$ salt.

for the [$Co^{II}Cl_4$]$^{2-}$ salt, 3.600(1) Å [Cl(2)···Cl(2)] for the [$Mn^{II}Cl_4$]$^{2-}$ salt, and 3.614(1) Å [Cl(2)···Cl(2)] and 3.649(1) Å [Cl(4)···Cl(4)] for the [$Zn^{II}Cl_4$]$^{2-}$ salt. The Cl···Cl contacts (<3.5 Å) were observed only in the [$Co^{II}Cl_4$]$^{2-}$ salt. The shortest S···Cl distances are 3.638(5) Å [S(11)···Cl(1)] for the [$Co^{II}Cl_4$]$^{2-}$ salt, 3.647(3) Å [S(17)···Cl(3)] for the [$Zn^{II}Cl_4$]$^{2-}$ salt, which are a little shorter than the van der Waals contact (3.65 Å), and 3.706(1) Å [S(11)···Cl(1)] for the [$Mn^{II}Cl_4$]$^{2-}$ salt. These results suggest that there could be a small interaction between π electrons of the donors and d spins of the magnetic metal anions. Heavily disordered EtOH molecules occupy the space surrounded by BDT-TTP columns and [$Mn^{II}Cl_4$]$^{2-}$ anions, and prevent the accurate determination of the structures. In general, the inclusion of crystal solvents is not desirable in the development of the molecular conductors because it tends to cause the localization of conduction electrons at low temperatures (Anderson localization). However, it seems that the crystals of organic conductors with divalent [$M^{II}Cl_4$]$^{2-}$ anions are apt to include solvent molecules (EtOH) because the organic conductors with similar tetrahalide transition-metal dianions, such as κ-(BETS)$_4$[$Co^{II}Cl_4$](EtOH), θ-(BETS)$_4$-[$Mn^{II}Br_4$](EtOH)$_2$,[11] and (BEDT-TTF)$_3$[$Mn^{II}Cl_3$]$_2$(EtOH)$_2$[10f] prepared from the PhCl or trichloroethane solution containing 10% EtOH, also contain EtOH as crystal solvents. This structural feature is considered to originate from the fact that the crystal lattice can be stabilized by the inclusion of solvent molecules because the crystal solvents separate the neighboring dianions and thus reduce the electrostatic repulsion between the dianions. It seems that crystal solvents (especially highly polarizable molecules such as EtOH)[17] are necessary to stabilize the crystal lattices of these dianion salts.

Electrical Properties. Figure 6 shows the temperature dependence of the electrical resistivities of the [$M^{II}Cl_4$]$^{2-}$ (M = Co, Mn, and Zn) salts. The salts exhibit similar room-

Table 3. The Intermolecular Short S···S Contacts (Å) of $(BDT\text{-}TTP)_3[M^{II}Cl_4](EtOH)_x$ (M = Co, Mn, and Zn; $x \approx 1.0$)[a)]

Direction	$(BDT\text{-}TTP)_3[Co^{II}Cl_4](EtOH)_x$[b)]	$(BDT\text{-}TTP)_3[Mn^{II}Cl_4](EtOH)_x$[b)]	$(BDT\text{-}TTP)_3[Zn^{II}Cl_4](EtOH)_x$
c1	none	none	S3···S10: 3.669
			S8···S16: 3.673
c2	S3···S7: 3.671	S2···S6: 3.689	S1···S9: 3.664
	S4···S8: 3.670	S3···S7: 3.688	S3···S11: 3.634
		S4···S8: 3.684	S4···S12: 3.626
			S5···S13: 3.683
			S6···S14: 3.607
c3	none	none	none
p1	S6···S10: 3.351	S6···S10: 3.351	S13···S20: 3.572
	S7···S10: 3.613	S7···S10: 3.666	S14···S19: 3.335
			S15···S18: 3.670
			S15···S19: 3.557
p2	none	none	none
p3	none	none	none
p4	S2···S9: 3.599	S2···S9: 3.551	S6···S23: 3.622
	S3···S9: 3.369	S3···S9: 3.363	S7···S23: 3.324
	S4···S12: 3.679	S4···S12: 3.689	
q1	S6···S10: 3.351	S6···S10: 3.351	S10···S22: 3.371
	S7···S10: 3.613	S7···S10: 3.666	S11···S22: 3.596
q2	none	none	none
q3	none	none	none
q4	S2···S9: 3.599	S2···S9: 3.551	S2···S18: 3.644
	S3···S9: 3.369	S3···S9: 3.363	S3···S18: 3.386
	S4···S12: 3.679	S4···S12: 3.689	

a) The intermolecular contacts c1, c2, c3, p1, p2, p3, p4, q1, q2, q3, and q4 are given in Fig. 5. b) p1, p2, p3, and p4 are symmetrically equal to q1, q2, q3, and q4, respectively.

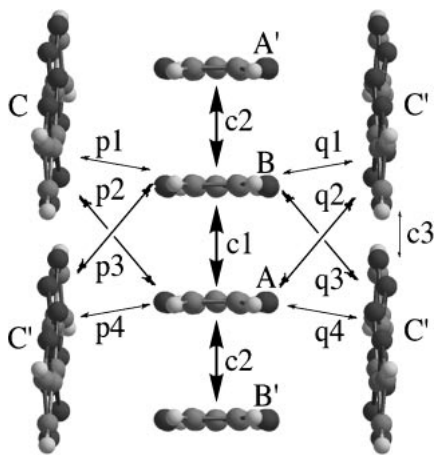

Fig. 5. Donor arrangement of $(BDT\text{-}TTP)_3[M^{II}Cl_4](EtOH)_x$ (M = Co, Mn, and Zn; $x \approx 1.0$) viewed along the molecular long axis. The intermolecular overlap integrals are presented in Table 4.

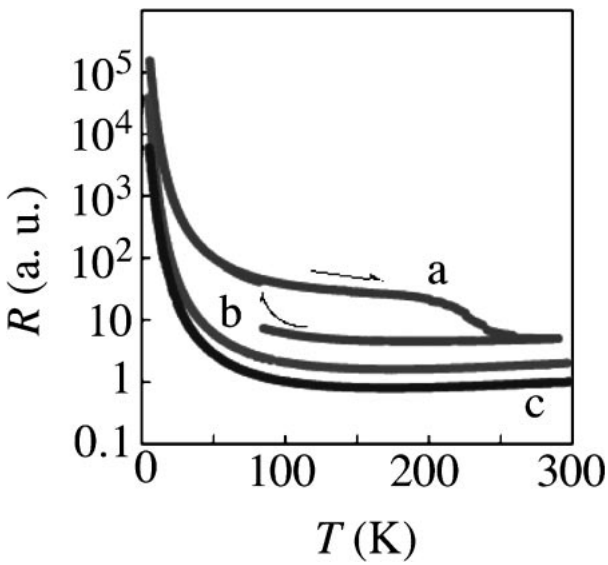

Fig. 6. Temperature dependence of electrical resistivities of $(BDT\text{-}TTP)_3[M^{II}Cl_4](EtOH)_x$ (M = Co, Mn, and Zn; $x \approx 1.0$): (a) the $[Co^{II}Cl_4]^{2-}$ salt, (b) the $[Mn^{II}Cl_4]^{2-}$ salt, and (c) the $[Zn^{II}Cl_4]^{2-}$ salt. The resistivity of each salt is shifted from the corrected one respectively for clarity. The room-temperature conductivity is about 5 S cm^{-1} for every salt.

temperature conductivities ($\sigma_{rt} \approx 5$ S cm^{-1}) and weakly metallic behavior. The resistivities decrease slowly with decreasing temperature and have a very shallow minima around 150 K. At low temperature the resistivities gradually increase, but the crystals retain high conductivities even around 30 K. The gradual resistivity increase at low temperature suggests the localization effect of π conduction electrons due to the lattice disorder (Anderson localization), which is consistent with the fact that the crystals contain heavily disordered crystal solvents. Except for the abrupt jump around at 85 K in the $[Co^{II}Cl_4]^{2-}$ salt probably due to a crack in the crystal, the resistivities showed no distinct anomaly down to liquid helium temperature.

Magnetic Properties. The temperature dependence of magnetic susceptibilities of the $[M^{II}Cl_4]^{2-}$ (M = Co, Mn, and Zn) salts was measured using a SQUID magnetometer. Figure 7 presents χT versus T plots of the $[M^{II}Cl_4]^{2-}$ (M = Co, Mn, and Zn) salts. In the $[Zn^{II}Cl_4]^{2-}$ salt, the data that were corrected for the 1% of paramagnetic impurity are presented. The $[Zn^{II}Cl_4]^{2-}$ salt without magnetic ions showed temperature-independent paramagnetism ($\chi \approx 7.5 \times 10^{-4}$ emu mol^{-1}), which is attributable to the Pauli-like paramagnetism of π conduction electrons. The relatively large temperature-independent paramagnetism seems to be consistent with the co-existence of two types of BDT-TTP chains along the *c* axis, that is, BDT-TTP stacks and BDT-TTP tapes. No distinct changes were observed down to 2.0 K, suggesting that the system could be essentially metallic down to low temperature. The temperature dependence of the magnetic susceptibility of the $[Co^{II}Cl_4]^{2-}$ and $[Mn^{II}Cl_4]^{2-}$ salts showed the contribution from π conduction electrons (temperature independent Pauli-like susceptibility of about 8×10^{-4} emu mol^{-1}) and that from the localized magnetic moments of transition-metal atoms (Curie–Weiss term). Curie–Weiss fittings give the Curie constants (C), Weiss temperatures (θ), and g-values as follows: $C = 2.25$ emu K mol^{-1}, $\theta = -1.6$ K, and $g = 2.2$ for the $[Co^{II}Cl_4]^{2-}$ salt, and $C = 4.26$ emu K mol^{-1}, $\theta = -0.8$ K, and $g = 2.0$ for the $[Mn^{II}Cl_4]^{2-}$ salt. These results suggest the magnetic ions of each salt to be in high-spin states ($S = 3/2$ for Co atom and $S = 5/2$ for Mn atom) and the very weak antiferromagnetic interactions between the anions. Thus, it is considered that π conduction electrons and high-spin localized magnetic moments coexist down to fairly low temperatures in these conductors. However, no sign of significant interactions between π electrons and localized d spins were observed.

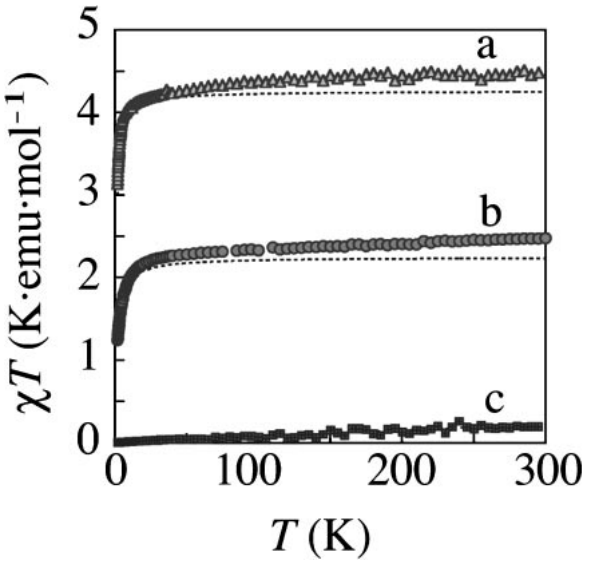

Fig. 7. Temperature dependence of χT value of (BDT-TTP)$_3$[$M^{II}Cl_4$](EtOH)$_x$ (M = Co, Mn, and Zn; $x \approx 1.0$): (a) the $[Mn^{II}Cl_4]^{2-}$ salt measured at 1 Tesla, (b) the $[Co^{II}Cl_4]^{2-}$ salt measured at 1 Tesla, and (c) the $[Zn^{II}Cl_4]^{2-}$ salt measured at 2 Tesla. The fitting curves for (a) the $[Mn^{II}Cl_4]^{2-}$ salt and (b) the $[Co^{II}Cl_4]^{2-}$ salt were calculated from the Curie–Weiss law [(a) $C = 4.26$ emu K mol^{-1}, $\theta = -0.80$ K and $g = 2.0$, and (b) $C = 2.25$ emu K mol^{-1}, $\theta = -1.6$ K and $g = 2.2$].

Band Structure Calculations. The extended Hückel-type tight-binding band structures of the $[M^{II}Cl_4]^{2-}$ (M = Co, Mn, and Zn) salts were calculated on the basis of the room-temperature structures. Needless to say, only the HOMOs of molecules A, B, and C were included. The intermolecular overlap integrals of the HOMO of BDT-TTP are shown in Table 4 and Fig. 5. As mentioned before, molecules A and B form an approximately regular column along the *c* axis, which is consistent with the fairly high conductivities of the systems. Of course, the interactions along this column are much larger than the other interactions, but fairly large interactions are found also between the adjacent C molecules. That is, there are two types of one-dimensional bands along the *c* axis. One is a wide band that originates from the BDT-TTP column and the other is a narrow band coming from the BDT-TTP tape. Owing to the fairly large interaction between the columns and the tapes (see Table 4 and Fig. 5), these bands are strongly modified. It is said that these salts have unique two-dimensional S···S networks and π conduction electrons can be delocalized over the two-dimensional network in the *bc* plane. The average charge of BDT-TTP molecules in these salts is +2/3, but the charge distribution over three independent BDT-TTP molecules (A,

Table 4. Intermolecular Overlap Integrals of HOMO, S ($\times 10^{-3}$) of (BDT-TTP)$_3$[$M^{II}Cl_4$](EtOH)$_x$ (M = Co, Mn, and Zn; $x \approx 1.0$)[a)]

Direction	(BDT-TTP)$_3$[$Co^{II}Cl_4$](EtOH)$_x$[b)]	(BDT-TTP)$_3$[$Mn^{II}Cl_4$](EtOH)$_x$[b)]	(BDT-TTP)$_3$[$Zn^{II}Cl_4$](EtOH)$_x$
c1	−29.0	−29.0	−27.9
c2	28.5	28.3	−25.4
c3	6.9	6.9	7.3
p1	−4.1	3.9	6.7
p2	2.0	−2.1	4.6
p3	−4.8	4.9	1.4
p4	7.0	−7.1	−7.7
q1	−4.1	3.9	−1.1
q2	2.0	−2.1	−4.6
q3	−4.8	4.9	−2.5
q4	7.0	−7.1	7.2

a) The intermolecular interactions c1, c2, c3, p1, p2, p3, p4, q1, q2, q3, and q4 are given in Fig. 5. b) p1, p2, p3, and p4 are symmetrically equal to q1, q2, q3, and q4, respectively.

B, and C) can be inhomogeneous. However, the obtained bond lengths could not provide any clear information on the formal charges of three BDT-TTP molecules. It may be said that π electrons in molecule C will feel the relatively low potential energy because molecule C occupies the interstitial position between π-donor columns consisting of molecules A and B, relatively close to the position of $[M^{II}Cl_4]^{2-}$ anion. In order to see the effect of the difference of site potential between the molecules, the tight-binding band calculations were made with changing the magnitude of the diagonal matrix element corresponding to molecule C ($\varepsilon_{HOMO} + \delta$), which means that the "effective site potential" of the π electron on molecule C is higher than those on molecules A and B by δ (the site potential on molecule A is assumed to be almost equal to that on B because molecules A and B form an approximately regular column). Figure 8 shows the density of state $D(\varepsilon)$ for $\delta = 0.0$, 0.21, 0.40, and 0.8 eV. To see the origin of the peaks of $D(\varepsilon)$ clearly, the band structure and the density of state were also calculated by neglecting the matrix elements between molecules A and C and molecules B and C, where the density of state $[D'(\varepsilon)]$ corresponds to the density of states of a hypothetical system consisting of isolated columns and isolated sheets. At first sight, the holes seem to be distributed equally on molecules A, B, and C for $\delta = 0.0$ ($A^{+2/3}B^{+2/3}C^{+2/3}$) because the π electron feels the same site potential on every BDT-TTP. However, as seen from $D'(\varepsilon)$, this is not true due to the difference in the band widths of the band of BDT-TTP column ($W \approx 1.2$ eV) and that of BDT-TTF tape ($w \approx 0.3$ eV) (see Fig. 8). The band-filling of the narrow band of BDT-TTP tape will become much larger than that of the wide band. The charge distribution estimated from the amplitude of the wave functions of the occupied states ($\varepsilon < \varepsilon_F$) was $A^{+0.85}B^{+0.85}C^{+0.30}$ for $\delta = 0.0$ eV. Despite the same site potential on every BDT-TTP, molecule C will be much more neutral than molecules A and B, which is inconsistent with the characteristic feature of the crystal structures mentioned above. For $\delta \approx 0.21$ eV, $D(\varepsilon)$ was found to be made up of two 2/3-filled bands (narrow band corresponding to BDT-TTP tape and wide band corresponding to BDT-TTP column), which means that the homogeneous charge distribution of $A^{+0.67}B^{+0.67}C^{+0.67}$ will be realized when the site potential on site C is about 0.2 eV higher than those on sites A and B. When $\delta = 0.40$ eV, the calculated state density indicated the charge distribution of $A^{+1/2}B^{+1/2}C^{+1}$. When $\delta > 0.70$ eV, $D(\varepsilon)$ consists of a vacant narrow band and a filled wide band, which means the holes are localized on molecules C, the charge distribution is expressed as $A^0B^0C^{+2}$. However, it would be not so usual if TTF-like π-donor molecules have formal charge near +2.0 and the one-dimensional compact stacking of neutral BDT-TTP molecules would be destabilized when there is no charge-transfer interaction along the *c* axis. In addition, the energy gap between the narrow band and wide band would make the system an insulator, which is inconsistent with the observed resistivity behavior. Thus, δ is considered to be 0.4 ± 0.2 eV. The energy dispersion curves are given in Fig. 9. Due to the interaction between narrow and wide bands, the dispersion curves were fairly modified around ε_F and the system has neither large Fermi surfaces nor band gap, which is consistent with the observed weakly metallic behavior.

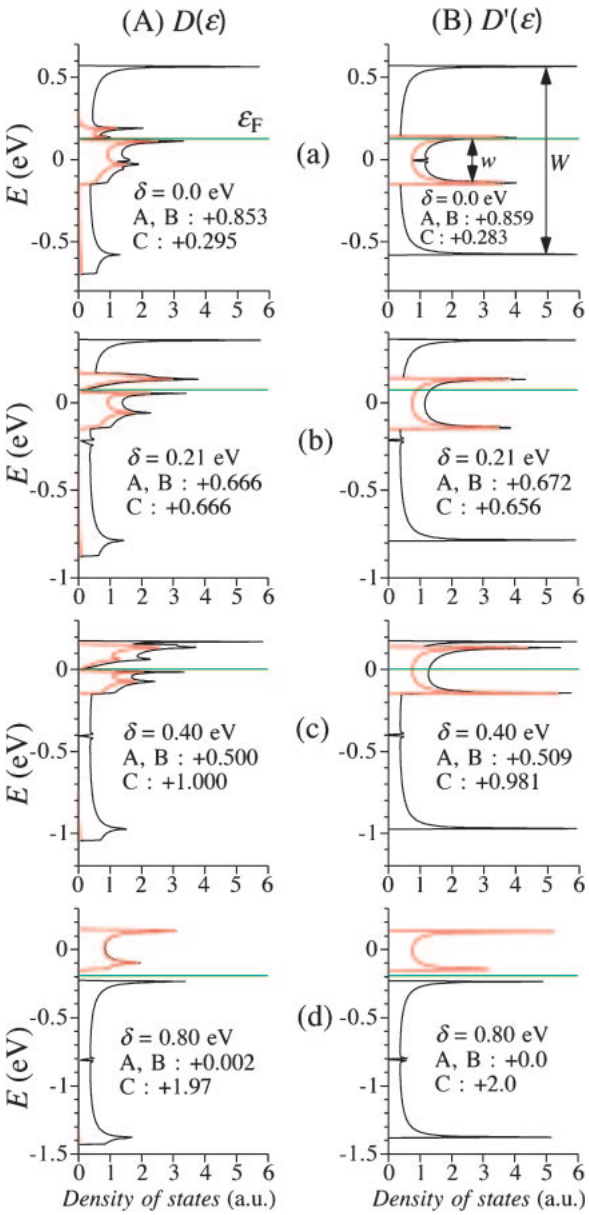

Fig. 8. The density of state $[D(\varepsilon)]$ of the tight-binding bands of $(BDT\text{-}TTP)_3[Mn^{II}Cl_4](EtOH)_x$ ($x \approx 1.0$). The density of state of the hypothetical lattice without intermolecular interactions between the BDT-TTP column (molecules A and B) and BDT-TTP sheet (molecule C) $[D'(\varepsilon)]$ was also calculated in order to see the nature of $D(\varepsilon)$. The value δ represents the difference of the site potential between molecule A (=molecule B) and molecule C and ε_F is Fermi energy. The red line indicates the "contribution of molecule C" to the density of state. The squared norm of corresponding components of molecule C in the eigen state with energy ε is summed up throughout the *k*-space and every band: $Contribution(\varepsilon) = \sum_{k,band(\varepsilon)} |a|^2$. For example, when δ is 0.40 eV, by comparing $D(\varepsilon)$ and $D'(\varepsilon)$ it is easily seen that the bands are composed of a 3/4-filled wide band and half-filled narrow band; that is, the charge distribution of $A^{+0.5}B^{+0.5}C^{+1}$ is suggested to be realized when $\delta \approx 0.4$ eV. $D(\varepsilon)$ is strongly reduced at $\varepsilon \approx \varepsilon_F$ by the interaction between the columns and the tapes.

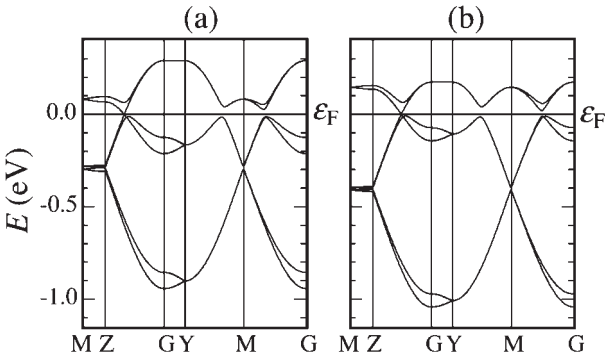

Fig. 9. Calculated band structures of $(BDT\text{-}TTP)_3[Mn^{II}Cl_4](EtOH)_x$ ($x \approx 1.0$) (see also Fig. 8). (a) All donors are equally oxidized ($A^{+0.67}B^{+0.67}C^{+0.67}$) ($\delta = 0.21$ eV). (b) Band structure for $\delta = 0.40$ eV corresponding to the approximate charge distribution of $A^{+0.5}B^{+0.5}C^{+0.1}$. These energy dispersion curves indicate that the system has a very small Fermi surface or almost zero-band gap irrespective of δ-value. The $[Co^{II}Cl_4]^{2-}$ and $[Zn^{II}Cl_4]^{2-}$ salts have almost the same band structures.

Conclusion

BDT-TTP based cation radical salts containing $[M^{II}Cl_4]^{2-}$ (M = Co, Mn, and Zn) anions were prepared. Single-crystal X-ray structure analyses revealed that each salt has a similar unique crystal structure and the D:A ratio of 3:1. The crystals contain two types of one-dimensional arrays of π molecules, that is, BDT-TTP columns and BDT-TTP tapes. The temperature dependence of the electrical resistivities of these salts showed weakly metallic behavior down to about 150 K. Despite the gradual resistivity increase at low temperature, every system retained fairly high conductivity, even at around 30 K. The gradual resistivity increase at low temperature originates from electron localization due to the lattice disorder. Magnetic measurements of the $[Zn^{II}Cl_4]^{2-}$ salt showed temperature independent Pauli paramagnetism. While the susceptibilities of the $[Co^{II}Cl_4]^{2-}$ and $[Mn^{II}Cl_4]^{2-}$ salts indicated the coexistence of the π conduction electrons and localized high-spins of Co^{II} and Mn^{II} atoms, however no interaction between π and d electrons could be observed. Extended Hückel tight-binding band structure calculations were performed by changing the site potential between the molecules in BDT-TTP columns and those in BDT-TTP tapes, which revealed the relation between the difference in the site potential and the possible charge distribution in the BDT-TTP lattice. Due to the interaction between the columns and the tapes, unique two-dimensional conduction networks were formed, which is consistent with the weakly metallic behavior of the crystal.

We thank Prof. Y. Misaki for his kind advice on the synthesis and crystal data of the BDT-TTP molecule. This study was partly supported by a Grant-in-Aid for Scientific Research on (S) (No. 14103005), Priority Areas of Molecular Conductors (No. 15073209), and for the 21st Century COE Program for Frontiers in Fundamental Chemistry from the Ministry of Education, Culture, Sports, Science and Technology. This work was also supported by CREST [Core Research for Evolutional Science and Technology of JST (Japan Science and Technology Agency)].

References

1 a) L. Ouahab, *Chem. Mater.* **1997**, *9*, 1909. b) F. Palacio, J. S. Miller, *Nature* **2000**, *408*, 421. c) M. Clemente-León, E. Coronado, J. R. Galán-Mascarós, C. Giménez-Saiz, C. J. Gómez-García, E. Ribera, J. Vidal-Gancedo, C. Rovira, E. Canadell, V. Laukhin, *Inorg. Chem.* **2001**, *40*, 3526.

2 a) L. Martin, S. S. Turner, P. Day, P. Guionneau, J. A. K. Howard, D. E. Hibbs, M. E. Light, M. B. Hursthouse, M. Uruichi, K. Yakushi, *Inorg. Chem.* **2001**, *40*, 1363. b) P. Day, M. Kurmoo, *J. Mater. Chem.* **1997**, *7*, 1291. c) A. W. Graham, M. Kurmoo, P. Day, *J. Chem. Soc., Chem. Commun.* **1995**, 2061. d) M. Kurmoo, A. W. Graham, P. Day, S. J. Coles, M. B. Hursthouse, J. L. Caulfield, J. Singleton, F. L. Pratt, W. Hayes, L. Ducasse, P. Guionneau, *J. Am. Chem. Soc.* **1995**, *117*, 12209. e) L. Martin, S. S. Turner, P. Day, F. E. Mabbs, E. J. L. McInnes, *Chem. Commun.* **1997**, 1367.

3 a) E. Coronado, J. R. Galán-Mascarós, C. J. Gómez-García, V. Laukhin, *Nature* **2000**, *408*, 447. b) A. Alberola, E. Coronado, J. R. Galán-Mascarós, C. Giménez-Saiz, C. J. Gómez-García, *J. Am. Chem. Soc.* **2003**, *125*, 10774.

4 a) A. Kobayashi, T. Udagawa, H. Tomita, T. Naito, H. Kobayashi, *Chem. Lett.* **1993**, 2179. b) H. Kobayashi, H. Tomita, T. Naito, A. Kobayashi, F. Sasaki, T. Watanabe, P. Cassoux, *J. Am. Chem. Soc.* **1996**, *118*, 368. c) H. Kobayashi, H. Akutsu, E. Arai, H. Tanaka, A. Kobayashi, *Phys. Rev. B* **1997**, *56*, R8526. d) H. Akutsu, E. Arai, H. Kobayashi, H. Tanaka, A. Kobayashi, P. Cassoux, *J. Am. Chem. Soc.* **1997**, *119*, 12681. e) H. Tanaka, A. Kobayashi, A. Sato, H. Akutsu, H. Kobayashi, *J. Am. Chem. Soc.* **1999**, *121*, 760. f) L. Brossard, R. Clerac, C. Coulon, M. Tokumoto, T. Ziman, D. K. Petrov, V. Laukhin, M. J. Naughton, A. Audouard, F. Goze, A. Kobayashi, H. Kobayashi, P. Cassoux, *Eur. Phys. J. B* **1998**, *1*, 439. g) E. Ojima, H. Fujiwara, K. Kato, H. Kobayashi, H. Tanaka, A. Kobayashi, M. Tokumoto, P. Cassoux, *J. Am. Chem. Soc.* **1999**, *121*, 5581. h) H. Fujiwara, E. Fujiwara, Y. Nakazawa, B. Z. Narymbetov, K. Kato, H. Kobayashi, A. Kobayashi, M. Tokumoto, P. Cassoux, *J. Am. Chem. Soc.* **2001**, *123*, 306. i) T. Otsuka, A. Kobayashi, Y. Miyamoto, J. Kiuchi, S. Nakamura, N. Wada, E. Fujiwara, H. Fujiwara, H. Kobayashi, *J. Solid State Chem.* **2001**, *159*, 407. j) H. Kobayashi, H.-B. Cui, A. Kobayashi, *Chem. Rev.* **2004**, *104*, 5265. k) H. Fujiwara, H. Kobayashi, *Bull. Chem. Soc. Jpn.* **2005**, *78*, 1181.

5 a) S. Uji, H. Shinagawa, T. Terashima, T. Yakabe, Y. Terai, M. Tokumoto, A. Kobayashi, H. Tanaka, H. Kobayashi, *Nature* **2001**, *410*, 908. b) L. Balicas, J. S. Brooks, K. Storr, S. Uji, M. Tokumoto, H. Tanaka, H. Kobayashi, A. Kobayashi, V. Barzykin, L. P. Gor'kov, *Phys. Rev. Lett.* **2001**, *87*, 067002.

6 a) H. Kobayashi, A. Sato, E. Arai, H. Akutsu, A. Kobayashi, P. Cassoux, *J. Am. Chem. Soc.* **1997**, *119*, 12392. b) A. Sato, E. Ojima, H. Akutsu, H. Kobayashi, A. Kobayashi, P. Cassoux, *Chem. Lett.* **1998**, 673. c) H. Kobayashi, A. Kobayashi, P. Cassoux, *Chem. Soc. Rev.* **2000**, *29*, 325.

7 a) B. Zhang, H. Tanaka, H. Fujiwara, H. Kobayashi, E. Fujiwara, A. Kobayashi, *J. Am. Chem. Soc.* **2002**, *124*, 9982. b) H. Fujiwara, H. Kobayashi, E. Fujiwara, A. Kobayashi, *J. Am. Chem. Soc.* **2002**, *124*, 6816.

8 a) R. R. Schumaker, E. M. Engler, *J. Am. Chem. Soc.* **1977**, *99*, 5519. b) Y. Misaki, H. Nishikawa, K. Kawakami, S. Koyanagi, T. Yamabe, M. Shiro, *Chem. Lett.* **1992**, 2321. c) Y.

Misaki, K. Kawakami, H. Nishikawa, T. Yamabe, M. Shiro, *Chem. Lett.* **1993**, 1337. d) Y. Misaki, private communication.

9 a) Y. Misaki, H. Fujiwara, T. Yamabe, T. Mori, H. Mori, S. Tanaka, *Chem. Lett.* **1994**, 1653. b) H.-B. Cui, T. Otsuka, A. Kobayashi, N. Takeda, M. Ishikawa, Y. Misaki, H. Kobayashi, *Inorg. Chem.* **2003**, *42*, 6114.

10 a) P. Day, M. Kurmoo, T. Mallah, I. R. Marsden, R. H. Friend, F. L. Pratt, W. Hayes, D. Chasseau, J. Gaultier, G. Bravic, L. Ducasse, *J. Am. Chem. Soc.* **1992**, *114*, 10722. b) A. Kobayashi, A. Sato, E. Arai, H. Kobayashi, C. Faulmann, N. Kushch, P. Cassoux, *Solid State Commun.* **1997**, *103*, 371. c) N. D. Kushch, O. A. Dyachenko, R. B. Lyubovskii, S. I. Pesotskii, M. V. Kartsovnik, A. E. Kovalev, P. Cassoux, H. Kobayashi, *Adv. Mater. Opt. Electron.* **1997**, *7*, 57. d) T. Naito, T. Inabe, K. Takeda, K. Awaga, T. Akutagawa, T. Hasegawa, T. Nakamura, T. Kakiuchi, H. Sawa, T. Yamamoto, H. Tajima, *Synth. Met.* **2001**, *120*, 877. e) T. Naito, T. Inabe, T. Akutagawa, T. Hasegawa, T. Nakamura, Y. Hosokoshi, K. Inoue, *Synth. Met.* **2003**, *135–136*, 613. f) T. Naito, T. Inabe, *J. Solid State Chem.* **2003**, *176*, 243. g) T. Mori, H. Inokuchi, *Bull. Chem. Soc. Jpn.* **1988**, *61*, 591.

11 E. Fujiwara, V. Gritsenko, H. Fujiwara, I. Tamura, H. Kobayashi, M. Tokumoto, A. Kobayashi, *Inorg. Chem.* **2002**, *41*, 3230.

12 CrystalStructure 3.10: *Crystal Structure Analysis Package*, Rigaku and Rigaku/MSC, **2000–2002**.

13 H.-B. Cui, T. Otsuka, A. Kobayashi, Y. Misaki, H. Kobayashi, *Bull. Chem. Soc. Jpn.* **2003**, *76*, 97.

14 Based on the unit cell volumes of the crystals of BETS, κ-(BETS)$_4$[Co^{II}Cl$_4$](EtOH) and (BETS)$_2$[Co^{II}Cl$_4$],[6c,11] the spaces occupied by [Co^{II}Cl$_4$]$^{2-}$ anion and EtOH molecule included in the crystal were roughly calculated to be about 107 and 140 Å^3, respectively. Then, the unit cell volumes of BDT-TTP and (BDT-TTP)$_3$[Co^{II}Cl$_4$](EtOH)$_x$ crystals suggested the space occupied by EtOH molecules to be about 590 Å^3, indicating $x \approx 1$.[8c] This stoichiometry was consistent with the result of X-ray structure refinement.

15 The optimization of the molecular structure of BDT-TTP was performed using the programs, MOPAC (PM3).

16 H. Kobayashi, A. Kobayashi, Y. Sasaki, G. Saito, H. Inokuchi, *Bull. Chem. Soc. Jpn.* **1986**, *59*, 301.

17 The dielectric polarizability of EtOH ($\varepsilon_r \approx 24.5$) is much larger than that of PhCl (5.7), which gives one of the reasons why dianion likes EtOH as a crystal solvent.